Journal of Power Sources 232 (2013) 376–388

Contents lists available at SciVerse ScienceDirect

Journal of Power Sources

journal homepage: www.elsevier.com/locate/jpowsour

Non-equilibrium two-phase model of the air-cathode of a PEM fuel cell based on GDL experimental water transport characteristics

Bladimir Ramos-Alvarado [a], Abel Hernandez-Guerrero [a], Michael W. Ellis [b,*]

[a] Department of Mechanical Engineering, University of Guanajuato, Mexico
[b] Department of Mechanical Engineering, Virginia Polytechnic Institute and State University, United States of America

HIGHLIGHTS

- Two computational models of the air-cathode of a PEMFC are developed using a two-phase approach.
- The novelty of the models is the application of experimentally determined properties of the GDL.
- Common empirical correlations for GDL behavior are shown to underpredict saturation.
- Experiments show that the model can predict performance based on measured GDL characteristics.

ARTICLE INFO

Article history:
Received 25 May 2012
Accepted 28 October 2012
Available online 24 November 2012

Keywords:
PEMFC
Modeling
Fuel cell
GDL
Capillary pressure
Numerical

ABSTRACT

In this work two models of the air-cathode of a PEM fuel cell are proposed using a two-phase non-equilibrium approach. The novelty of both models is that they use experimentally determined porosity, capillary pressure relationships, and permeability of the gas diffusion material in order to demonstrate whether or not the use of these properties enhances the accuracy of PEM fuel cell models to predict performance curves and liquid water saturation distribution. The first model is a 1-D model, where the effect of using experimental water transport properties of the GDL is assessed in terms of water saturation distribution in the GDL. The second model is a 2-D model used to predict experimental polarization curves. It was found that the implementation of the experimentally determined water transport characteristics of the GDL predicts more liquid water saturation than using empirical correlations for the capillary pressure curves and permeability. It was also observed that polarization curves of two cells using different GDL material can be predicted accurately using the appropriate GDL properties.

1. Introduction

PEM fuel cell modeling has been employed for many years, as an effective way to design, improve, and predict the performance of these devices. Accurate modeling is not an easy task due to the two-phase phenomena exhibited by operating PEM fuel cells, namely the liquid water transport and the reactant gas transport through the porous GDL. There are three approaches to study the two-phase flow in the porous media of the fuel cell: (1) the pore network approach is based on stochastic procedures to generate a network of pores, aiming to reproduce the intricate matrix of a GDL to predict the functional relationship of the water transport characteristics [1–4]; (2) the direct method which is based on a microscopic treatment of the GDL in which the actual structure of the porous media is reconstructed by microscopic imaging [5]; and finally, (3) the continuum medium approach which is widely applied in the literature and has many advantages over the other methodologies, including the capability to provide a complete cell-level model and low computing time compared to higher fidelity approaches.

Continuum models refer to the traditional models broadly used in many applications involving a flow through a porous media; some applications include petroleum engineering and subsurface hydrology. The porous medium is treated as a hypothetical effective continuum and the models involve volume-averaged quantities such as saturation and rely on phenomenological relationships such as the generalized Darcy's law. Key parameters in this approach are the permeability, relative permeability and the capillary pressure-saturation curve [1].

Two main modeling schemes can be distinguished in the continuum models. The first one was proposed by Wang and Chen [6]. These authors presented a novel formulation of the

* Corresponding author. Tel: +1 (540) 231-9102.
E-mail address: mwellis@vt.edu (M.W. Ellis).

0378-7753/$ – see front matter © 2012 Elsevier B.V. All rights reserved.
http://dx.doi.org/10.1016/j.jpowsour.2012.10.091

transport processes based on a multicomponent system for porous media. The model equations developed include mass conservation, momentum conservation, species transport, and the energy equation. The multi-phase mixture model is commonly referred as the M^2 model. One of the main features of the M^2 model is that the two-phase stream (gas–liquid) is treated as a single stream by introducing averaged mixture properties and variables in the governing equations. This model has been widely employed, from its initial development [7] on transport of organic compounds, until more recent applications to PEM fuel cells two-phase models [8–17].

Alternatively to the M^2 method, there is a simpler model often referred as the multi-fluid-model or MFM. This method is based on solving the conservation equations for the liquid phase and the gas phase separately using source and sink terms to account for mass exchange among phases. The MFM has been widely reported in the literature when dealing with two-phase flow analysis in PEMFCs [18–35]. In the MFM, Darcy's equation is applied in the GDL to each phase. It is usually assumed that the gas phase pressure gradient is negligible; this assumption is called the unsaturated flow theory or UFT. The UFT has been applied in most of the work that uses the MFM approach. With this assumption, the gradient of the capillary pressure is equal to the negative of the liquid phase pressure gradient:

$$\nabla P_c = \nabla P_g - \nabla P_l = -\nabla P_l \tag{1}$$

as a result, the liquid phase transport equation in the GDL is transformed to:

$$\nabla\cdot(\rho_l \vec{u}) = \nabla\cdot\left(-\frac{\rho_l K}{\mu_l}\nabla P_l\right) = \nabla\cdot\left(\frac{\rho_l K}{\mu_l}\nabla P_c\right) = 0 \tag{2}$$

where κ is the effective permeability of the liquid phase, namely, the absolute permeability, K (a property of the porous media), times the relative permeability of the liquid phase, k_{rl} (a function of the flow conditions, the porous matrix, the saturation of the pores with liquid water, etc.). Using the chain rule, the gradient of the capillary pressure can be expressed as a function of saturation knowing that there is a functional relationship $P_c(s)$:

$$\nabla\cdot\left[\rho_l\left(\frac{K k_{rl}}{\mu_l}\frac{dP_c}{ds}\right)\nabla s\right] = 0 \tag{3}$$

where the quantity inside the inner parenthesis is often called the liquid water diffusion coefficient D_w.

So far, the two common approaches applied to the analysis of two-phase flow in PEMFCs have been briefly described. A comparison between these two approaches was addressed by Pasaogullari and Wang [9]. They presented a 1D model of the cathode side GDL of a PEMFC where the flow channels and the catalyst layer were considered as boundary conditions. The only equation solved in [9] was the liquid mass transport equation using both approaches, UFT and M^2 model. Pasaougullari and Wang found that the UFT under predicts saturation in comparison with the M^2 approach; they, also found that the oxygen distribution in the GDL was also underpredicted by the UFT. The water saturation obtained by the UFT was slightly below the M^2 prediction; on the other hand, the oxygen distribution did show a considerable difference. The pressure distribution of the gas phase was compared using both methods and a deviation of 2 kPa at 2 A cm^{-2} in a GDL of 0.3 mm thick was observed.

Regardless of the approach used to simulate water transport through the porous media of a PEM fuel cell, two constitutive relationships are necessary: the capillary pressure-saturation relationship and the liquid phase relative permeability-saturation relationship. These expressions are necessary due to the capillary transport mechanism of the liquid water in the GDL. Table 1 shows some of the first assumptions found in the literature for the functional relationships required for a continuum model. He et al. [18] just assumed a constant liquid water diffusion coefficient and a linear function for the relative permeability of the liquid water. Nartarajan and Nguyen [19] proposed an expression for the gradient of the capillary pressure curve where the constants were adjusted via experimental polarization curves and the relative permeability was defined as a linear function of saturation Wang et al. [8] were one of the first groups to use a modification of the empirical Leverret function for well-sorted sand to evaluate the capillary pressure-saturation relationship in a PEM fuel cell GDL. These empirical relationships are written in terms of reduced saturation (S) instead of saturation (s). In order to simplify the modeling efforts, Nam and Kaviany evaluated the slope of the Leverret function in the range $0 < S < 0.5$ to represent the capillary pressure curve relationship. Pasaogullari et al. [12], proposed a modified form of the Leverret function to describe the effects of having a hydrophobic or hydrophilic porous media.

The modification of the empirical Leverret correlation for well-sorted sand proposed by Pasaogullari et al. [12] and the liquid phase relative permeability empirical relationship for the same material have been widely used among researchers involved in the modeling of PEM fuel cells. The popularity of this method can be seen in the large number of modeling articles referring to the Leverret function and the cubic expression for relative permeability of the liquid phase as the most appropriate or simplest manner to address the effects of capillary motion of liquid water through the GDL. The disadvantage to this approach is that it is not well-connected to measurable characteristics of the GDL material

Table 1
Different expressions found in the literature for capillary pressure and liquid water relative permeability relationships.

$P_c(s)$ relationship	k_{rl} (liquid phase relative permeability)	Reference
$D_w = 1\times10^{-4}\ \mathrm{cm^2\,s^{-1}}$	$k_{rl} = s$	[18]
$\frac{dP_c}{ds} = -A\times D[e^{-A(s-C)} + e^{A(s-C)}]$	$k_{rl} = s + 0.01$	[19]
$P_c = \frac{\sigma\cos\theta}{(K/\varepsilon)^{1/2}}[1.417(1-S) - 2.12(1-S)^2 + 1.236(1-S)^3]$	$k_{rl} = S^3$	[8]
$\frac{dP_c}{dS} = 30321$ [Pa] Slope of Leverret function $0 \le S < 0.5$	$k_{rl} = S^3$	[20]
$P_c = \frac{\sigma\cos\theta}{(K/\varepsilon)^{1/2}}J(S)$ $J(s) = \begin{cases} 1.417S - 2.12S^2 + 1.262S^3 & \theta \ge 90^\circ \\ 1.417(1-S) - 2.12(1-S)^2 + 1.262(1-S)^3 & \theta < 90^\circ \end{cases}$	$k_{rl} = S^3$	[12]

and hence cannot provide insight into how GDL characteristics affect performance. In this work, the experimental characterization performed on carbon paper Toray 090 by Ramos-Alvarado et al. [36] is taken as the base of two numerical models of the air-cathode of a PEM fuel cell. First, a 1-D model is developed aiming to show that the empirical Leverret function and relative permeability correlation for well-sorted sand are inappropriate when liquid water saturation distribution is predicted for carbon paper under different wet-proof treatments. The second model is a 2-D representation of the cathode side of a PEM fuel cell operating at very high stoichiometric conditions. The objective of the 2-D model is to predict polarization using different GDL materials with different water transport properties and compares the predictions with experimental polarization curves.

2. Model development

In this section, the modeling efforts followed to assess the impact of using experimentally determined water transport characteristics to predict liquid water saturation and polarization in a PEMFC are presented. First, a 1-D model of the air-cathode of a PEM fuel cell is developed to study the distribution of liquid water saturation. This model was run using the widely used empirical correlations for well-sorted sand and with the experimentally determined capillary pressure curves and relative permeability functions obtained in [36]. Secondly, a 2-D model of the air-cathode of a PEMFC is developed to predict experimental polarization behavior. This 2-D model is run using experimentally determined water transport characteristics and electrochemical parameters including exchange current density, open circuit voltage, and the transfer coefficient.

2.1. Modeling assumptions

The simplifications implemented to the 1-D model are listed below.

1. Steady state operation of the fuel cell.
2. Isothermal operation.
3. Liquid water is introduced at the catalyst layer-GDL interface due to the cathode electrochemical reaction and due to electro-osmotic drag from the anode.
4. The gas phase pressure is constant, which means a null gas phase pressure gradient throughout the domain. The UFT assumption is applied.
5. No irreducible saturation is present in the gas diffusion media.
6. There is no equilibrium of phases between liquid water and water vapor (i.e. water can move between phases).
7. A 1D model approach is appropriate to compare the effects of using different constitutive relations in the prediction of liquid water saturation distribution.

For the development of the 2-D model, the assumptions from 1 to 6 were taken, except that the 2-D model considers a non-isothermal operation. The 2-D analysis is based on reactant and product concentrations at a particular point along the flow channel and assumes that the change in composition along the flow channel is negligible (i.e. operation with a high stoichiometric ratio).

2.2. Computational domains

Fig. 1 shows the cross-section of a PEMFC. Both sides components, anode and cathode, are shown. The effect of compression of the current collector over the gas diffusion media is depicted, as well as the catalyst layers and the polymeric electrolyte membrane.

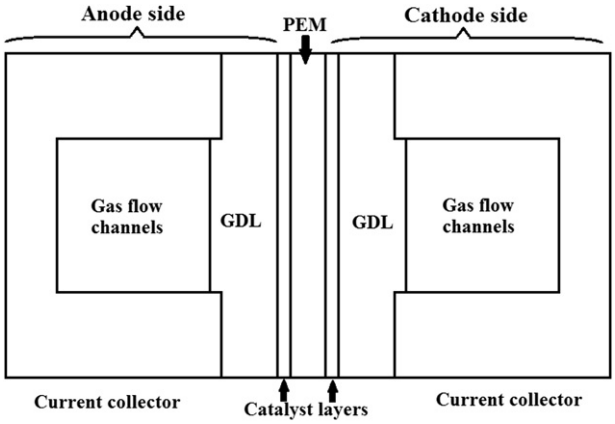

Fig. 1. Cross-section of a PEMFC.

The models developed will study only the cathode side of the fuel cell due to the higher activation barrier of the cathode reactions in comparison with the anode reactions. The computational domains will be described in the following paragraphs.

The computational domain of the 1-D model consists of the one-dimensional length through plane of the cathode GDL. Fig. 2 shows the geometry studied. The boundaries of this model are the interface with the catalyst layer ($x = 0$) and the interface with the gas flow channel ($x = L$). In this model $L = 287$ μm, which is the average thickness of the gas diffusion media studied.

In order to simplify the numerical computations in the 2-D model, a discrete region is taken as computational domain; see Fig. 3. The computational domain consists of two subdomains: (1) D_1 is the PEM and (2) D_2 is the GDL, both subdomains are half of the cross-section shown in Fig. 1. In this computational domain, the catalyst layer was reduced to an interface between subdomains D_1 and D_2. The effects of the catalyst layer will be considered in the electrochemistry of this model. The dimensions shown in Fig. 3 are: (1) the uncompressed thickness of the gas diffusion layer under the gas flow channels (x_u); (2) the compressed thickness of the gas diffusion layer under the collector plate (x_c); (3) the in plane length of the uncompressed GDL (y_u); (4) the in plane length of the compressed portion of the GDL (y_c); and (5) the PEM thickness (x_m).

2.3. Governing equations

Table 2 shows the governing considered in the analysis as well as information regarding the application of such equations.

Given that air is the reactant gas in the cathode, Eq. (4) represents three equations, one for each component: O_2, H_2O, and N_2; however, only two equations are solved, O_2 and H_2O, and the mass fraction of N_2 is calculated by:

$$\sum_{i=1}^{n} \omega_i = 1 \tag{9}$$

The source term in Eq. (4) accounts for species consumption or generation in the computational domain. In this model, only water goes through phase change and is modeled by [18]:

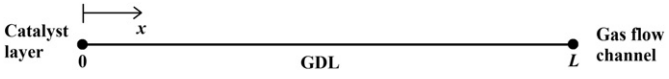

Fig. 2. 1-D model computational domain.

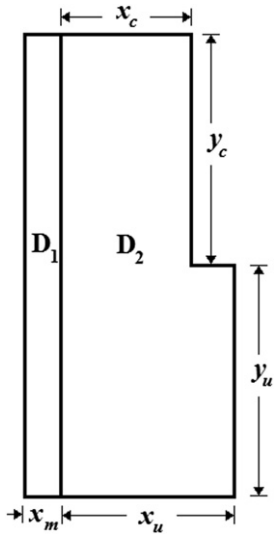

Fig. 3. 2-D model computational domain, dimensions and subdomains.

$$r_{H_2O} = k_c \frac{\varepsilon(1-s)x_{H_2O}}{RT}\left(x_{H_2O}P - P^{sat}_{H_2O}\right) q + k_e \frac{\varepsilon s \rho_l}{M_{H_2O}}\left(x_{H_2O}P - P^{sat}_{H_2O}\right)(1-q) \quad (10)$$

where k_c and k_e are the condensation and evaporation constants, s is the local liquid water saturation, P is the pressure of the mixture, $P^{sat}_{H_2O}$ is the saturation pressure, T is the absolute temperature in K, x_{H2O} is the molar fraction of water vapor, M_{H2O} is the water molar mass, ρ_l is the liquid water density, and q is the switch function that allows to change between condensation and evaporation:

$$q = \frac{1}{2} + \frac{1}{2}\frac{\left|x_{H_2O}P - P^{sat}_{H_2O}\right|}{x_{H_2O}P - P^{sat}_{H_2O}} \quad (11)$$

Water vapor is either consumed or generated due to phase change in the air-cathode of a PEMFC. Oxygen is consumed at the catalyst layer interface only. Nitrogen, on the other hand, does not react at all in the computational domain; thus, a flow stagnation condition can be established in this component, allowing to calculate the bulk velocity of the gas mixture as:

Table 2
Governing equations.

Equation	Mathematical expression		1-D Model	2-D Model
Species transport	$\nabla\cdot\left(\rho_g\omega_i\vec{u} - \rho_g\omega_i\sum_{j=1}^{n}\tilde{D}_{ij}\frac{M_g}{M_j}\nabla\omega_j\right) = r_i$	(4)	✓	✓
Liquid water transport	$\nabla\cdot\left(\frac{\rho_l K k_{rl}}{\mu_l}\frac{dP_c}{ds}\nabla s\right) = r_l$	(5)	✓	✓
Energy	$\nabla\cdot\left(\rho_g c_p \vec{u}T - k_T^{eff}\nabla T\right) = r_T$	(6)		✓
Electric potential field	$\nabla\cdot(\sigma_e\nabla\phi_e) = 0$	(7)	✓	✓
Protonic potential field	$\nabla\cdot(\sigma_i\nabla\phi_i) = 0$	(8)		✓ (D_1)

$$\vec{u} = \frac{1}{\rho_g\omega_{N_2}}\left(\rho_g\omega_{N_2}\sum_{j=1}^{n}\tilde{D}_{ij}\frac{M_g}{M_j}\nabla\omega_j\right) \quad (12)$$

In order to ensure conservation of mass between the liquid water evaporating (from the liquid phase) and the water vapor gained (to the gas phase) or the liquid water condensating (to the liquid phase) and the water vapor lost (from the gas phase), the source term of Eq. (5) is defined as:

$$r_l = -r_{H_2O} \quad (13)$$

The diffusivity of species was calculated using a symmetric multicomponent Fick model. In order to use this multicomponent model, the Maxwell–Stefan binary diffusivity is determined by:

$$D_{ij} = \frac{k_D T^{1.75}}{P\left(v_i^{1/3} + v_j^{1/3}\right)^2}\left(\frac{1}{M_i} + \frac{1}{M_j}\right)^{1/2} \quad (14)$$

where k_D is a constant equal to 3.16×10^{-8} Pa m^2/s, T is the absolute temperature in K, M_i is the molar mass of species i in kg/mol, P is the pressure expressed in Pa, and v_i equals the molar diffusion volume of species i expressed in m^3/mol. The effective Maxwell–Stefan diffusivities are calculated as suggested in [20]:

$$D_{ij}^{eff} = D_{ij}\left[\varepsilon\left(\frac{\varepsilon - 0.11}{1 - 0.11}\right)^{0.785}\right](1-s)^2 \quad (15)$$

In Eq. (15), the term inside the square brackets accounts for the effect of the reduction of diffusion due to porosity of the GDL, and the second term accounts for the reduction of diffusivity due to a partially saturated GDL with liquid water. At the end, the effective diffusivities are arranged in a symmetric matrix used to calculate the multicomponent Fick diffusivities.

In the energy equation, the source term, r_T, represents the thermal effect of phase change, and is calculated as:

$$r_T = r_{H_2O}\Delta h_{fg} \quad (16)$$

where Δh_{fg} is the water enthalpy of phase change. In the energy equation, the term k_T^{eff} represents the effective thermal conductivity of the computational domain, namely, carbon, liquid water, and humid air:

$$k_T^{eff} = (1-\varepsilon)k_{carbon} + \varepsilon s k_l + \varepsilon(1-s)k_g \quad (17)$$

The current density is calculated using:

$$j = j_o(1-s)\frac{c_{O_2}}{c_{O_2}^{ref}}\exp\left(\frac{\alpha n F}{RT}\eta_{act}\right) \quad (18)$$

where j_o is the exchange current density, c_{O2} is the concentration of oxygen at the catalyst layer interface, $c_{O_2}^{ref}$ is the reference concentration of oxygen, F is Faraday's constant, α is the transfer coefficient and relates to the symmetry of the reaction, n is the number of electrons transferred in the electrochemical reactions, and η_{act} is the activation overpotential given by:

$$\eta_{act} = V_{oc} - V_{cell} - \eta_{ohm} \quad (19)$$

where V_{oc} is the reversible cell voltage or open circuit voltage, V_{cell} is the actual cell voltage, and η_{ohm} is the ohmic overpotential which is calculated as the summation of the GDL and membrane loses:

$$\eta_{ohm} = 2\eta_{GDL} + \eta_{PEM} \quad (20)$$

where the GDL overpotential is assumed to be similar for anode and cathode side, η_{GDL} is calculated as the electric potential drop and η_{PEM} is the protonic potential drop in the PEM. It can be seen that η_{ohm} includes the effect of the PEM overpotential only in the 2-D model.

2.4. Boundary conditions

The boundary conditions applied to the 1-D model are summarized in Table 3.

Fig. 4 shows all the boundaries defined in the 2-D model developed where B_1 is the catalyst layer reduced to an interface, B_2 is the interface with the gas flow channel, B_3 and B_4 are the interfaces with the current collector plate, B_5 is the symmetry plane at the midpoint of the collector shoulder, B_6 is the symmetry plane at the midpoint of the flow channel, and B_7 the interface between the anode side of the fuel cell and the PEM. Table 4 summarizes the boundary conditions set at each boundary.

Symmetry conditions where defined at boundaries B_5 and B_6. At B_7 the protonic potential was defined as the corresponding anode potential, namely $\phi_i = 0$. At B2, the mass fractions $\omega_{O_2,GFC}$ and $\omega_{H_2O,GFC}$ are calculated based on air relative humidity supplied as reactant to the cathode.

2.5. Parameters and operating conditions of the model

The parameters employed in the numerical model are listed in Table 5.

The properties of carbon paper Toray 090 were taken from Ref. [36]. Two capillary pressure curves, one for non-wet-proofed material (untreated) and one for a GDL material with 20% of PTFE were fitted as shown in Fig. 5.

Table 6 presents the properties of the GDL material that was characterized in [36], properties that are going to be used in the numerical models.

2.6. Numerical procedures

COMSOL's default solver was used for the solution of the governing equations. A direct method was selected to solve the stationary problems (1-D and 2-D) using the MUMPS solver. The parallel sparse direct linear solver MUMPS (MUltifrontal Massively Parallel Sparse Direct Solver) works on general systems of the form $Ax = b$. MUMPS uses several preordering algorithms to permute the columns and thereby minimizing the fill-in. MUMPS is multithreaded on platforms that support multithreading and also supports solving on distributed memory architectures through the use of MPI. MUMPS also includes out-of-core capabilities. The MUMPS out-of-core solver stores the LU factors on the hard drive.

Table 3
1-D model boundary conditions

Equation	GDL–catalyst layer interface	GDL–gas flow channels interface
Oxygen transport	$\dot{m}_{O_2} = -M_{O_2}\frac{j}{4F}$	$\omega_{O_2} = \frac{1-\omega_{H_2O}}{1+r_{N_2/O_2}}$
Water vapor transport	$\dot{m}_{H_2O} = 0$	$\omega_{H_2O} = \frac{M_{H_2O}}{M_g}\frac{P^{sat}_{H_2O}}{P_g}RH$
Liquid water transport	$\dot{m}_l = M_{H_2O}\frac{j}{2F}(1+2\alpha_{net})$	$\dot{m}_l = h_m(s - s_{GFC})$
Electric potential field	$-\hat{n}\cdot(\sigma_e\nabla\phi_e) = -j$	$\phi_e = V_{cell}$

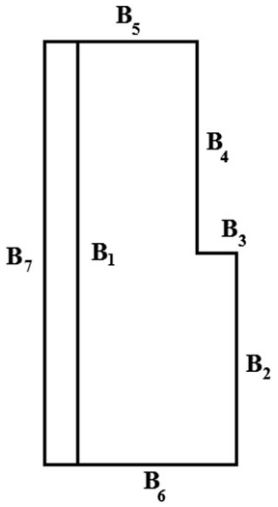

Fig. 4. Boundaries of the 2-D model.

This minimizes the internal memory usage. The price to pay is longer solution times because it takes longer time to read and write to disk than using the internal memory [37].

3. Experimental techniques

A commercial Ion Power Inc., Nafion catalyst coated membrane was used as MEA. Both sides of this coated membrane have a platinum content of 0.3 mg cm^{-2}. Two different GDL materials were used: Toray-090 untreated (without wet proofing) and the same material with a PTFE content of 20% (wet proofing 20% wt). The gasket material used was PTFE coated fiber glass. A single serpentine pattern served as gas distributor. The total length of the serpentine is 322 mm with square-shaped channels of 1 mm. The total active area of this assembly is 4.84 cm^2.

The test conditions were determined so that a high stoichiometric flow was attained. By using a high stoichiometric ratio, the depletion effects in the channels are not that important; hence, the 2-D mathematical model developed is suitable for describing the cell phenomena. The experimental test conditions are listed in Table 7.

Following the construction of the test cells, these were installed in a commercial fuel cell test station manufactured by Fuel Cell Technologies Inc.

3.1. Repeatability of experiments

After reaching a steady state operation of the test cells under the conditions described in the last section, the polarization curves were obtained. Three different experiments were conducted by varying the recording time of current at constant voltage conditions. Recording times of 20, 30, and 40 s were tested and are named as Experiment 1, Experiment 2, and Experiment 3 respectively. Fig. 6 shows the repeatability achieved during the experimentation with the two different single cells assembled. The polarization curves for the three experiments were found to be very similar, in each cell. Such results demonstrate a good repeatability of the experimental procedures.

3.2. Polarization curves and Tafel plot

Fig. 7 shows that the fuel cell using an untreated (non-wet-proofed) GDL material presents a higher performance than the fuel

Table 4
2-D model boundary conditions.

Equation	B_1	B_2	B_3, B_4
Oxygen transport	$\dot{m}_{O_2} = -M_{O_2}\frac{j}{4F}$	$\dot{m}_{O_2} = h_D(\omega_{O_2} - \omega_{O_2,GFC})$	$\dot{m}_{O_2} = 0$
Water vapor transport	$\dot{m}_{H_2O} = 0$	$\dot{m}_{H_2O} = h_D(\omega_{H_2O} - \omega_{H_2O,GFC})$	$\dot{m}_{H_2O} = 0$
Liquid water transport	$\dot{m}_l = M_{H_2O}\frac{j}{2F}(1 + 2\alpha_{net})$	$\dot{m}_l = h_m(s - s_{GFC})$	$\dot{m}_l = 0$
Energy	$-\hat{n}\cdot(\rho_g c_p \vec{u}T - k_T^{eff}\nabla T) = f_T(V_{oc} - V_{cell})j$	$q'' = h_T(T - T_o)$	$T = T_{cell}$
Electric potential field	$-\hat{n}\cdot(\sigma_e\nabla\phi_e) = j$	$-\hat{n}\cdot(\sigma_e\nabla\phi_e) = 0$	$\phi_e = V_{cell}$
Protonic potential field	$-\hat{n}\cdot(\sigma_i\nabla\phi_i) = -j$	N/A	N/A

Table 5
Numerical model parameters.

Description	Symbol	Value	Units
Mass ratio of N_2 to O_2	r_{N_2/O_2}	3.2917	–
Isobaric gas pressure	P_g	101.325	kPa
Cell temperature	T_{cell}	353	K
GDL porosity	ε	Varies with material	–
Net water transfer coefficients	α_{net}	0.5	–
Condensation constant	k_c	100	s^{-1}
Evaporation constant	k_e	1	$atm^{-1}\,s^{-1}$
Mass convection coefficient	h_m	1000	$kg\,m^{-2}\,s^{-1}$
Heat transfer convection coefficient	h_T	1.13	$W\,m^{-2}\,K^{-1}$
Diffusive convection coefficient	h_D	Varies with species	$kg\,m^{-2}\,s^{-1}$
Carbon thermal conductivity	k_{carbon}	6.75	$W\,m^{-1}\,K^{-1}$
Liquid water thermal conductivity	k_l	0.58	$W\,m^{-1}\,K^{-1}$
Gas phase thermal conductivity	k_g	0.02	$W\,m^{-1}\,K^{-1}$
Specific capacity of the gas phase	c_p	1008	$J\,kg^{-1}\,K^{-1}$
Heat partition factor	f_T	0.7	–

cell using wet-proofed material. These results may look controversial in regards to what is expected from the PTFE treatment, namely, a better water management in the cathode side; nevertheless, the following must be considered: (1) it was demonstrated that the material with 20% of PTFE has a very low permeability in comparison with a compressed non wet-proof material [36]; such a characteristic leads to a reduced diffusion of fuel in the anode side, likewise, it leads to a low diffusion of oxygen in the cathode side; (2) the operating conditions used in the experiments encourage good water removal, namely, the cathode relative

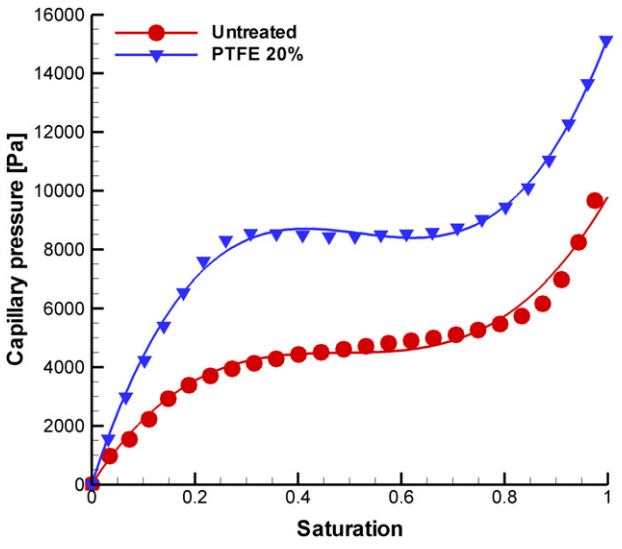

Fig. 5. Curve fitting to experimental capillary pressure curves taken from Ref. [36].

Table 6
Experimentally determined properties of carbon paper Toray 090 [36].

Material	$P_c(s)$ relationship [Pa]	k_{rl}	K [m^2]	ε
Untreated	$\frac{dP_c}{dS} = (2.7322 - 11.634S + 11.487S^2)\times 10^4$	S^5	8.236×10^{-12}	0.78
20% PTFE	$\frac{dP_c}{dS} = (5.3907 - 21.641S + 20.8519S^2)\times 10^4$	S^2	1.098×10^{-12}	0.73

humidity inlet condition was 70%; (3) the high frequency resistance of the cells was measured as 0.0968 Ω cm^2 and 0.1113 Ω cm^2, for the cell using non-wet-proofed and for the cell using wet-proofed GDL respectively; and (4) the hydrophobic characteristics of the GDL reduces the amount of moisture in the MEA and thus its conductivity is reduced. These arguments aid to explain the behavior observed in Fig. 7; further, there are references in the technical literature that support these findings [38–41].

Wet-proofing the GDLs leads to a better water removal but also decreases the gases diffusivity and the electric conductivity of the material; thus, an optimal PTFE content is expected to exist to account for this trade-off. However, there are many answers to this problem in the literature. Velayutham [38] found an optimal value of 35% PTFE content in terms of peak power density; however, this experimental work was conducted only in the micro-porous layer. Park et al. [39] found an optimal value of PTFE of 10% also in the micro-porous layer. Jie-Cheng and Chien-Kung [40] conducted a wide study at different humidity temperatures and at different PTFE loadings in the GDL and in the MPL. They found an optimal content of 40% PTFE in the GDL and 30% PTFE in the MPL at low humidity conditions. Park et al. [41] conducted a study addressing the effect of PTFE content in the GDL (Toray 090) on cell performance at different cell and gases temperatures. The work presented in [41] includes operating conditions very similar to those used in this work. Park et al. determined that, at operating conditions like the ones used in this study, the optimal PTFE content is 10% followed by 0%, and for PTFE contents of 20% and up, the cell performance decreases. This short literature review on the effect of wet-proofing in GDL material on cell performance is presented with the objective to show: (1) that no clear trends are observed in regards to the effect of GDL wet-proofing and cell performance, and (2) that there are authors reporting similar trends of cell performance like the ones presented here, under similar operating conditions and using the same GDL material.

Table 7
Experimental test conditions.

Parameter	Value	Units
Anode flow rate	225	sccm
Cathode flow rate	550	sccm
Cell temperature	353	K
Anode gas temperature	323	K
Cathode gas temperature	343	K
Anode/cathode back-pressure	0	Pa

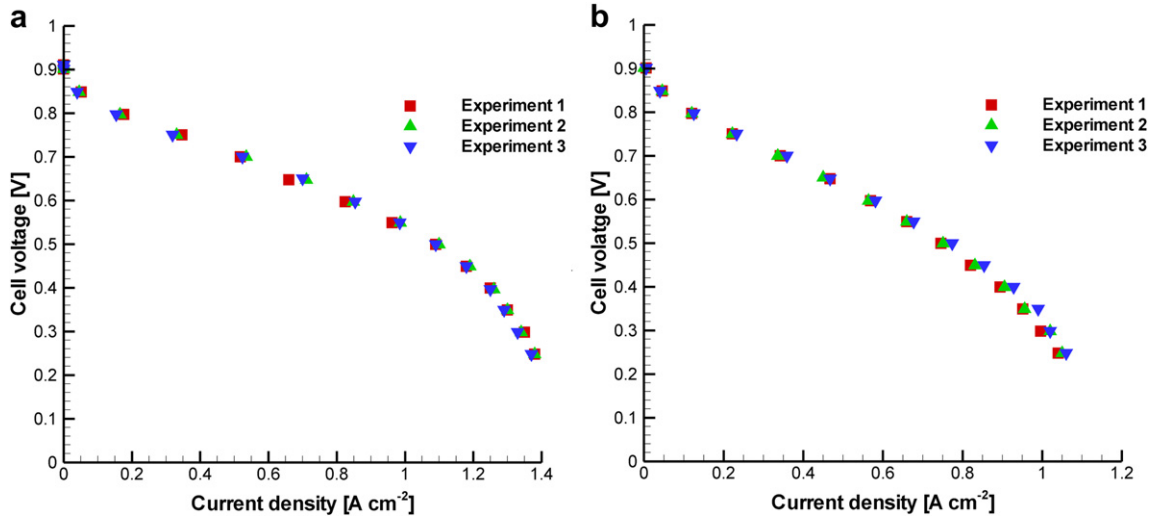

Fig. 6. Repeatability of experiments, polarization curves. (a) Single cell with an untreated GDL. (b) Single cell with a GDL with 20% of PTFE.

The Tafel plot was obtained for both test cells by calculating the logarithm of low current densities in the activation region of the polarization curves; however, the plots were similar due to the fact that similar MEA material (from the same stock) was used in both cells. The resulting Tafel plot is shown in Fig. 8. The electrochemical parameters calculated from this plot are $j_o = 49.5\ \mathrm{A\,m^{-2}}$ and $\alpha n = 1.223$.

4. Results

In this section, the 1-D modeling efforts are presented. This model was developed aiming to assess the impact of using experimentally determined capillary pressure functions and relative permeability functions on water saturation profiles across the gas diffusion media. In order to conduct this comparison, the widely reported empirical Leverett correlation and the empirical correlation for liquid water relative permeability for well-sorted sand ($k_{rl} = S^3$) was implemented and compared to the model using experimental data.

The 2-D modeling results are presented in this section. First, the properties of a compressed non-wet-proofed GDL will be used in the numerical model to see if polarization can be predicted. Later, the properties of a compressed wet-proofed GDL are going to be used as inputs of the numerical model in order to determine if by changing these properties, polarization can be predicted accurately.

4.1. 1-D model results

The properties of a compressed non-wet-proofed (untreated) material were implemented into a 1-D model using the properties and operating conditions shown in Table 5 and the GDL properties shown in Table 6. A different 1-D model was studied by only changing the capillary pressure function to the Leverett function, see Table 1 [12], and using $k_{rl} = S^3$ to describe relative permeability. The saturation profiles obtained are compared in Fig. 9(a) at an operating condition of $1\ \mathrm{A\,cm^{-2}}$.

It can be clearly seen that the empirical correlations of the type that have been widely used in the literature underpredict saturation in the GDL. In general, by using the experimental water transport characteristics, the water saturation prediction is nearly

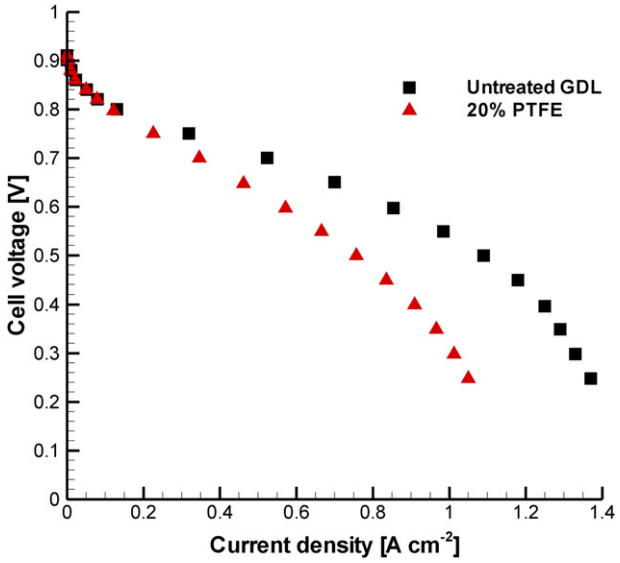

Fig. 7. Polarization curves of single cells using different GDL material.

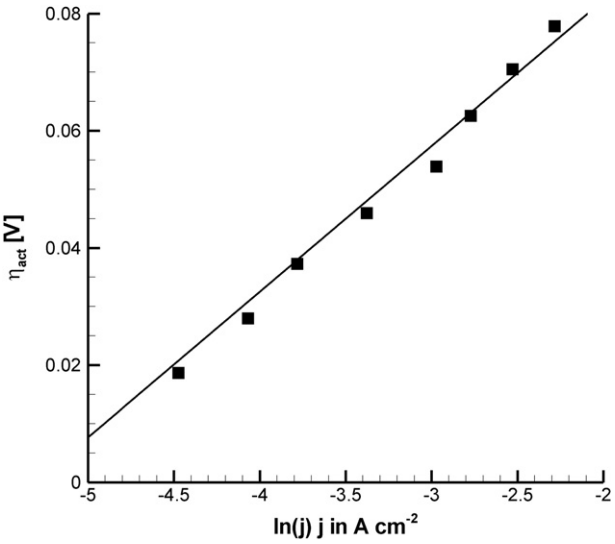

Fig. 8. Tafel plot.

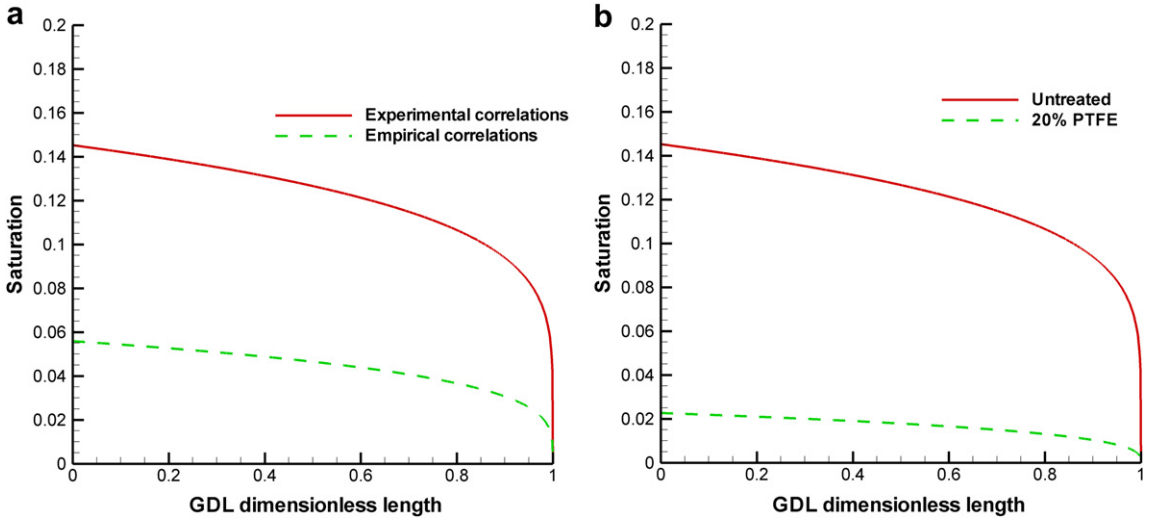

Fig. 9. Prediction of saturation profiles in the GDL. (a) Comparison between experimental and empirical correlations. (b) Comparison using experimental correlations for untreated and wet-proofed GDL.

twice than the water saturation predicted using empirical correlations. It can be observed that the water saturation is greater near the catalyst layer. This is due to the liquid water generation by the electrochemical reactions. The saturation profiles show a decrease near the gas flow channels where water is removed by convective mechanisms.

The effect of wet-proofing on the saturation profiles is depicted in Fig. 9(b). The effect of a wet-proofing treatment with of 20% (PTFE) is remarkable. Fig. 9(b) shows that the maximum saturation using the material with 20% of PTFE exhibits a maximum saturation of 2.4% whereas an untreated material shows a maximum saturation of 14.6%. Such an effect is attributed to the hydrophobic characteristics given to the GDL material by the PTFE treatment (wet-proofing).

A parametric study of liquid water saturation profiles on untreated compressed GDL is presented in Fig. 10. This study is conducted in order to assess the reliability of the response of the model to different operating conditions. Fig. 10(a) is a parametric study of the effect of the inlet air relative humidity on water saturation profiles at an operating condition of 1.4 A cm^{-2}. It is observed that as the relative humidity condition in the cathode increases, the saturation increases due to the high water content in the air stream. This high water concentration in the air leads to a reduced evaporation rate and condensation is more likely to occur. On the other hand, as shown later in this section, low humidity conditions drive a larger evaporation rate. Fig. 10(b) shows a parametric study of water saturation distribution at a constant relative humidity condition of 95% and a ranges of current density values. It can be observed in Fig. 10(b) that at larger current densities, the water saturation level increases. Such a behavior is obvious because the water production is directly proportional to the current density. By comparing Fig. 10(a) and (b) it can be inferred that the operating current density operating condition has a greater impact on water saturation than that of the inlet air relative humidity.

Fig. 11 presents a parametric study of oxygen distribution in a compressed and untreated GDL. Fig. 11(a) shows a study of the effect of inlet air relative humidity on oxygen distribution at

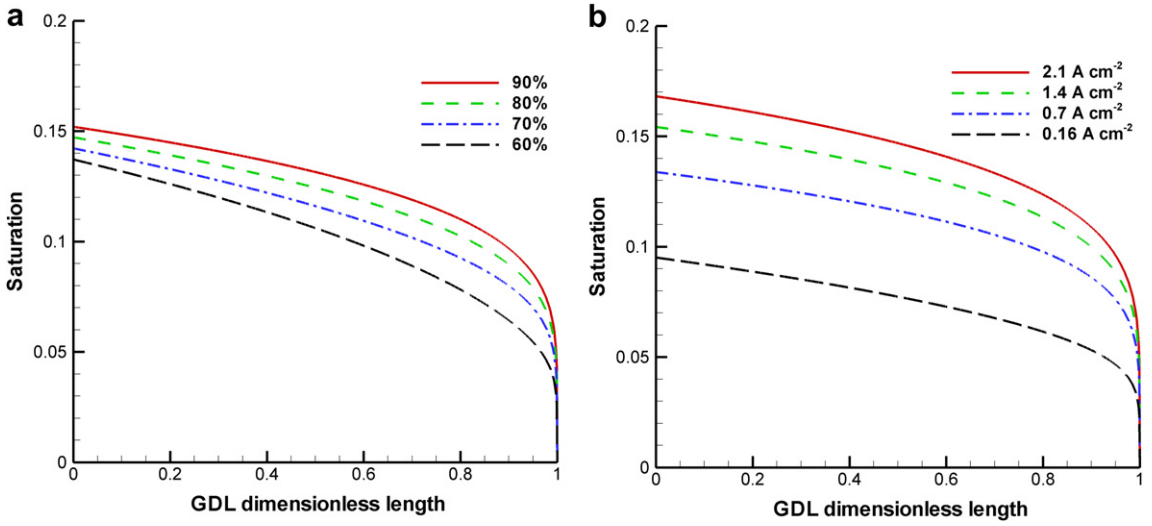

Fig. 10. Parametric study of liquid water saturation profiles in the GDL. (a) Cell operating at 1.4 A cm^{-2}. (b) Air inlet relative humidity of 95%.

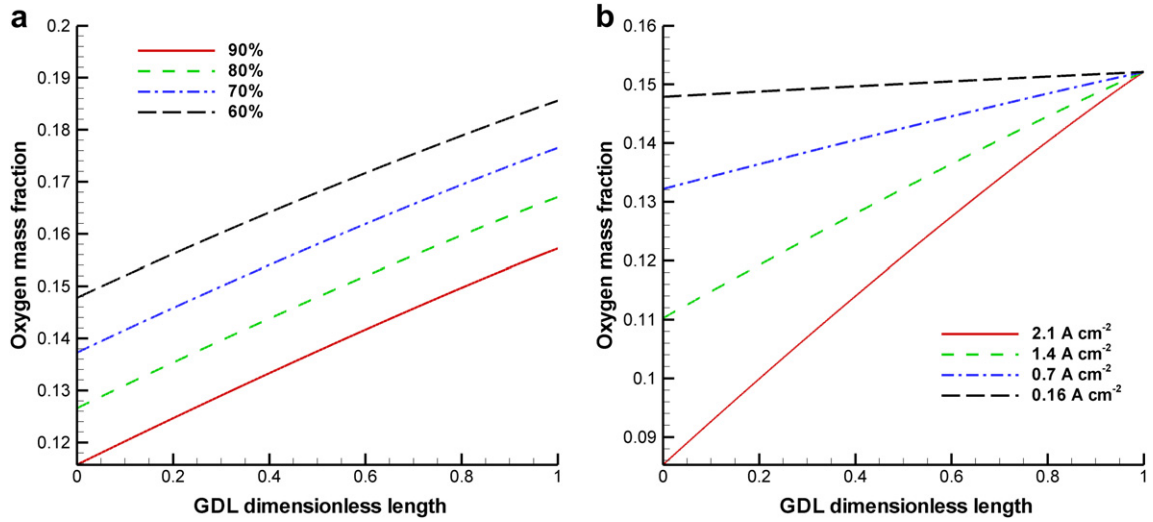

Fig. 11. Parametric study of oxygen distribution in the GDL. (a) Cell operating at 1.4 A cm^{-2}. (b) Air inlet relative humidity of 95%.

a constant current density. Relative humidity plays an important role when determining the concentration of oxygen and water vapor in humid air. Having a high relative humidity condition means a lower concentration of oxygen in humid air; conversely, a low humidity represents mixture with a higher concentration of oxygen. Fig. 11(b) shows a parametric study of oxygen concentration at a constant inlet air relative humidity condition of 95% and varying current density. As current density increases, the consumption of oxygen increases and thus the concentration gradient which drives diffusion must increase. It can be seen that at low current densities like 0.16 A cm^{-2} the gradient of oxygen across the GDL is not that considerable as that of an operating condition of 2.1 A cm^{-2}.

Whereas oxygen is consumed at the interface between the catalyst layer and the GDL, this interface is impermeable to water vapor. Fig. 12(a) shows the effect of inlet air relative humidity on water vapor distribution. All the curves shown have a different starting point at the gas flow channels interface that corresponds to the inlet humidity condition defined for each case. It is observed that water vapor mass fraction increases in direction from the gas flow channels interface towards the interface with the catalyst layer. The increase in water vapor mass fraction is due to the evaporation that takes place inside the GDL as predicted by the phase change model used (see Eq. (10)). The driving mechanism of phase change in this model is the non-equilibrium between phases. A measure of this non-equilibrium is given by the difference between the local water vapor pressure and the saturated vapor pressure at the local temperature. It can be seen how the gain in mass fraction is larger for low humidity (and hence low vapor pressure) conditions.

Fig. 12(b) shows the effect of different current density operating conditions on water vapor mass fraction distribution. All the cases studied share a common value at the interface with the flow channel because the relative humidity condition in the gas flow channels is the same. Water vapor mass fraction shows a tendency to increase as the current density increases. This can be explained by looking at the oxygen contours of Fig. 11(b). Oxygen concentration decreases as current density increases due to the increasing consumption rate, thus, due to the non-reactivity of nitrogen then the water vapor concentration must increase.

The parametric studies presented so far on saturation and species distribution have shown some important capabilities of the

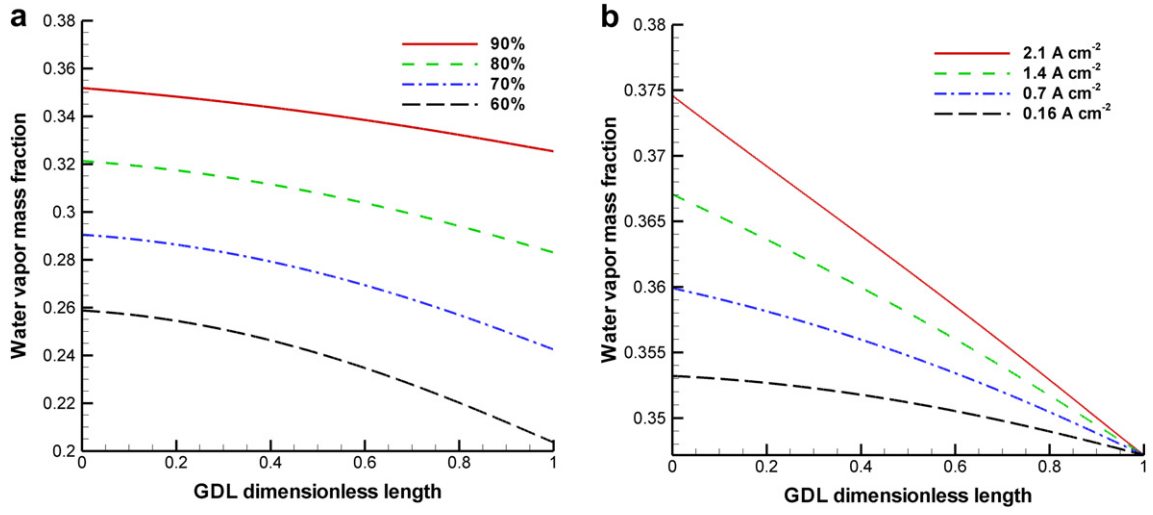

Fig. 12. Parametric study of water vapor distribution in the GDL. (a) Cell operating at 1.4 A cm^{-2}. (b) Air inlet relative humidity of 95%.

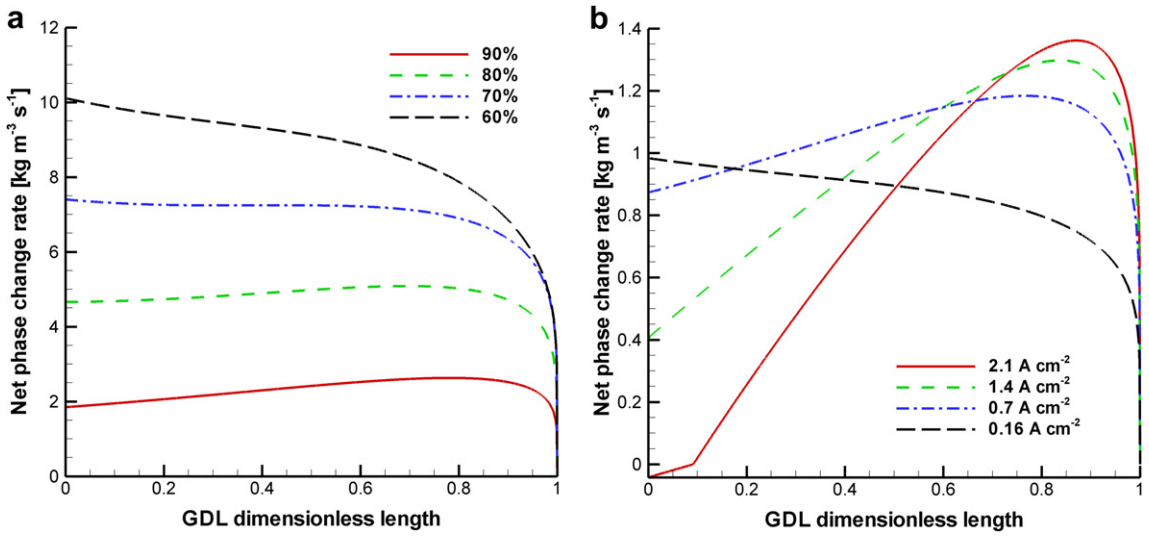

Fig. 13. Parametric study of the net phase change rate in the GDL. (a) Cell operating at 1.4 A cm^{-2}. (b) Air inlet relative humidity of 95%.

model developed. However, results like the ones presented in Fig. 11 would be better explained by looking at the phase change rates in the computational domain. Furthermore, it is interesting to look at how the phases interact inside the GDL. Fig. 13 shows a parametric study of the phase change rate in the GDL. According to the phase change model (Eq. (10)), the phase change driving mechanism is the non-equilibrium between local vapor pressure and the saturated vapor pressure at the local temperature. The convention of the present modeling efforts is that a positive phase change rate represents a gain in water vapor (evaporation) and a negative phase change rate represents condensation. It can be observed in Fig. 13(a) that the higher evaporation rate is for a condition of 60% relative humidity and the tendency is to reduce the evaporation rate as the inlet relative humidity condition increases. The curves depicted in Fig. 13 show a slight tendency to reduce the magnitude of evaporation rate in the regions close to the catalyst layer interfaces; such a behavior is due to the increase in relative humidity near the catalyst layer due to the higher content of liquid water. Another important feature observed in the curves of Fig. 13 is that they resemble the saturation profiles shown in Fig. 10. This is because the phase change model depends upon the existence of saturation in order to have evaporation. Condensation can occur at regions saturated with liquid water but only if the relative humidity is higher than 1.

The results shown in Fig. 13(a) predict that only evaporation occurs at the operating conditions studied. Fig. 13(b) shows how the model evolves from evaporation to condensation at a fixed high inlet humidity condition (95%) while current density is increased. At the lower current density condition, 0.16 A cm^{-2}, the phenomenon inside the GDL is purely evaporative; however, as the current density condition increases, liquid water saturation and local relative humidity increases from the gas flow channels interface to the catalyst layer interface. These phenomena create the peak shown in the curves and then the decrease of phase change rate to a condensation condition at the highest current density condition.

Local relative humidity profiles were obtained from the parametric studies shown previously. Fig. 14 shows profiles of local relative humidity at different operating conditions. Fig. 14(a) shows a tendency to increase the local relative humidity from the

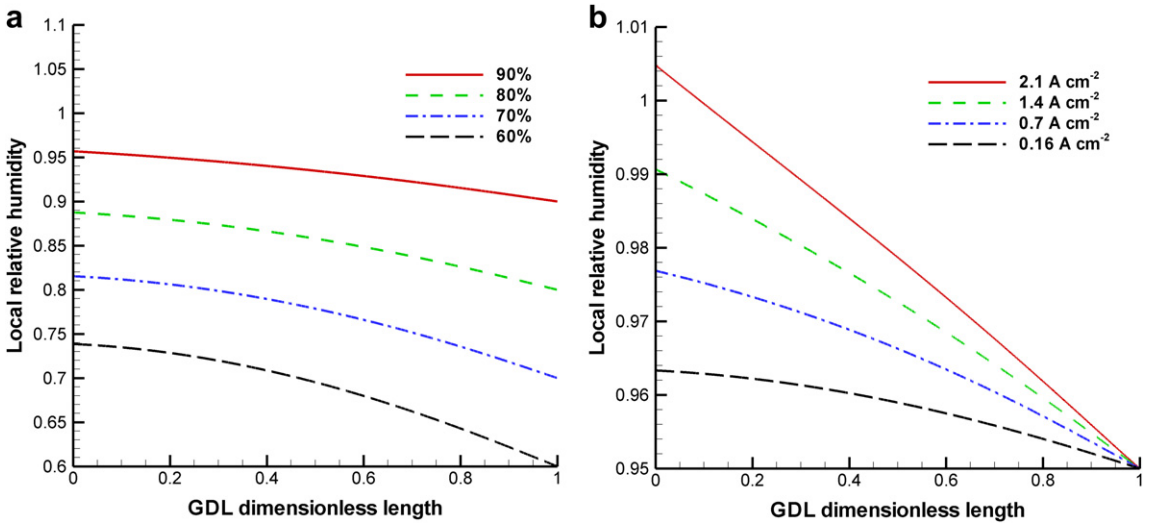

Fig. 14. Parametric study of local relative humidity in the GDL. (a) Cell operating at 1.4 A cm^{-2}. (b) Air inlet relative humidity of 95%.

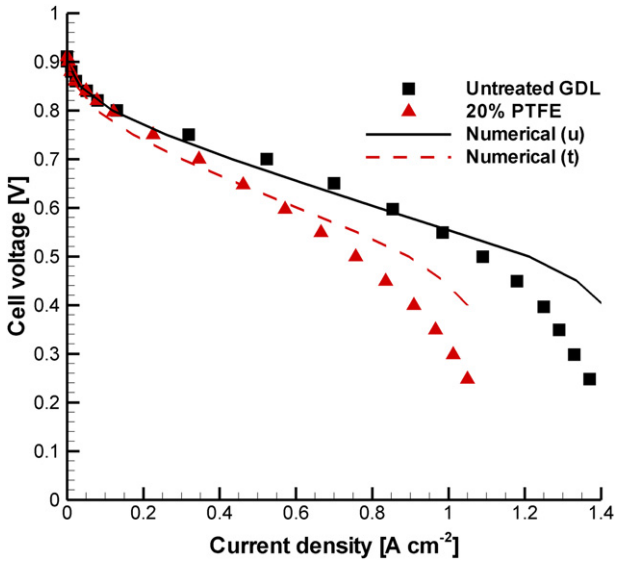

Fig. 15. Polarization prediction of fuel cells using different GDL materials.

gas flow channel interface to the catalyst layer interface. Such an increase in relative humidity is most likely attributed to the consumption of oxygen and the consequent increase of concentration of water vapor. The increase of relative humidity is also related to evaporation (see Fig. 13(a)) due to the high driving mechanism for this phase change phenomenon at low humidity conditions in the gas flow channels. The amount of relative humidity gain is reduced as the gas flow channel humidity condition increases. Fig. 14(b) shows that local relative humidity increases in the vicinity of the catalyst layers as the average current density increases. This is explained because oxygen is depleted faster at higher current densities, water vapor concentration increases, and therefore relative humidity increases too. Due to the high humidity condition in the gas flow channels, the phase change rate that depends upon relative humidity gradients turns from evaporation to condensation, see Fig. 13(b). That phenomenon can be explained by looking at Fig. 14(b). It is observed how at 2.1 A cm^{-2}, the local relative humidity is greater than 1, hence, the condensation phenomenon substitutes evaporation near the catalyst layer interface.

4.2. 2-D model results (validation)

It is commonly observed that the objective of most of the numerical models developed for fuel cells is to predict polarization behavior. Currently, models reported in the literature generally use a two-phase approach and most of them, report to predict polarization adequately although the models are based on *assumed* properties of the GDL material and also *assumed* electrochemical parameters. The novelty of the model presented in this work is to predict polarization by using actual experimentally determined properties of the GDL material and experimentally obtained electrochemical properties as well. In Section 3.2 two polarization curves were obtained for a cell assembled using non-wet-proofed and wet-proofed GDL material. The same MEA material was taken from the same stock and the cells were tested at the same operating conditions.

The main objective of this work is to determine if polarization curves can be predicted by using experimentally determined water transport properties of the GDL material, given that many of the most significant losses occur within this region of the cell, namely, diffusion of species, liquid water saturation of electrodes, and electric charge transfer. This hypothesis was tested and the steps followed are summarized here: (1) two cells were assembled using different GDL material (treated and untreated with PTFE) and in such a way that a compression of ~20% was obtained for the GDL material; (2) the water transport characteristics of GDL materials at compressions of ~20% were obtained experimentally [36]; (3) data from the GDLs and the Tafel plot (electrochemical parameters) were implemented in a numerical model of the air-cathode of a PMEFC to obtain the polarization curves of each cell. Fig. 15 presents a comparison between experimental polarization curves

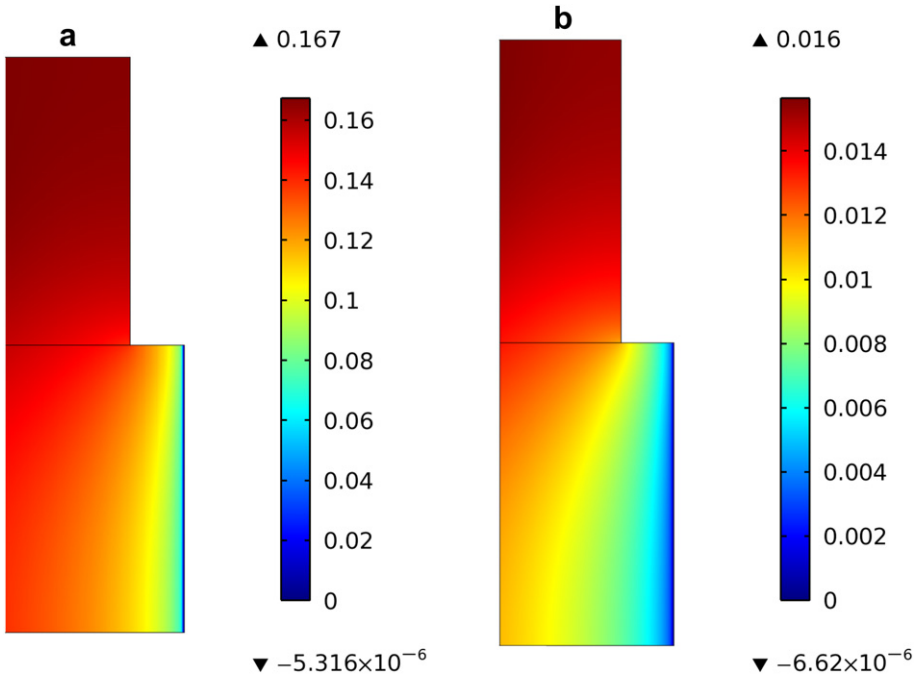

Fig. 16. Saturation contours of liquid water saturation. (a) Non-wet-proofed GDL. (b) Wet-proofed GDL.

and the polarization curves predicted using the numerical 2-D model developed. It can be clearly seen that a good prediction of polarization was obtained using the numerical model. The three overpotential zones are observed in the numerical model results; however, the concentration zone is where both numerical results, for the untreated and the wet-proofed GDL model, differ with the experimental data. Actually, this region was very difficult to calculate beyond an operating condition of 0.4 V due to divergence of the solution process.

Under high current density conditions (e.g., > 0.9 A cm^{-2}) the concentration loss effects become more significant for both fuel cells. At this high current density condition liquid water is produced at high rates and has partially saturated the electrode. As seen in the following section, saturation is particularly high under the shoulders of the collector plates. Sole [42] has suggested that this area under the collector plate shoulder exhibits the lowest contact resistance and that excessive saturation in a region that would otherwise produce the highest current, has a more detrimental effect than is predicted by models which assume a uniform contact resistance over the surface of the MEA. This rationale may explain why models such as the one presented here (which does not address variations in contact resistance) overpredict cell performance at very high current density.

Fig. 16 presents liquid water saturation contours for both cells, using untreated and treated GDL materials at an operating condition of 1 A cm^{-2}. The saturation contours for the different materials are shown using different scale due to the considerable differences between both saturation levels. It can be observed that the cell using non-wet-proofed material presents more saturation than the cell using wet-proofed material, such a result was expected and makes sense. In spite of the differences between the magnitudes of saturation levels, similar characteristics can be observed and will be discussed here. It is observed in both cases shown in Fig. 16 that the lowest saturation levels occur near the interface with the gas flow channels. This is evident because at that interface, the gas stream removes liquid water by a convective mechanism. It is also observed that the highest liquid water saturation levels are present in the region below the land (under the current collectors). Such an accumulation of water can be explained due to the impermeability of the current collector to the water, and due to the long pathway between the water generated below the land and the interface with the gas flow channels.

5. Conclusions

Much of the continuum modeling approaches for PEM fuel cells reported in the literature use empirical correlations for materials like well-sorted sand as inputs to the water transport equation. Only recently has research been conducted and reported in the literature in regards to the characterization of GDL material in order to provide actual water transport properties such as capillary pressure, porosity, and permeability. In the present work such properties were taken from experimentally reported data for carbon paper Toray 090 [36].

Experimental performance was obtained for fuel cells using untreated GDL material and also using treated GDL material with 20% of PTFE. It is well known that wet-proofing is applied to increase performance of the cell by avoiding electrode flooding. However, it is also reported in the literature that the amount of wet-proofing must be optimized for the intended operating conditions. In the experiments conducted here (at low humidity conditions) it was observed that the cell using an untreated GDL performed better than the cell using a wet-proofed GDL. These results were attributed to the (1) reduction of the pore space due to the PTFE content in the GDL; (2) creation of a more tortuous path due to the PTFE treatment; (3) reduction of the GDL conductivity due to the PTFE sintered in the carbon fibers of the GDL; and (4) reduction of MEA humidification due to the hydrophobic GDL used in the anode and cathode side. From these experiments, electrochemical parameters such as the transfer coefficient, the exchange current density, and the operating cell voltage were determined for the MEA material used.

Experimental characterization data of GDL material and electrochemical parameters determined for the MEA material were used as inputs of two numerical models of a PEMFC. A 1-D model was developed in order to assess the effect of using experimental water transport characteristics of a GDL on liquid water saturation distribution. The liquid water saturation profiles obtained using experimentally determined properties of the GDL were compared to those calculated using the most commonly used empirical correlations reported in the literature. It was found that the empirical correlations underpredict saturation levels in the GDL. The effect of wet-proofing was also studied and a remarkable reduction of saturation level was observed at the operating conditions simulated. A parametric study was conducted to demonstrate the reliability of the numerical model to predict species distribution and water saturation. The results obtained from this parametric study confirmed an appropriate description of the physics governing the operation of PEM fuel cells.

At the end and as a closing study, a 2-D model was developed seeking to replicate the polarization curves obtained using different GDL material. It was observed that by varying the water transport characteristics of the GDL, a good agreement between experimental and numerical data was attained for current density as high as 1 A cm^{-2}. With these results, it was demonstrated that polarization of PEM fuel cells using different GDL material can be predicted just by using adequate GDL and water transport properties. Further investigation of the capabilities of the numerical model was conducted by obtaining saturation distribution in the regions below the current collectors and under the gas flow channels. It was found that the liquid water saturation is higher under the land of the current collectors than under the channels. Such results were expected and match with other works reported in the literature.

Acknowledgments

This work was conducted at the Institute for Critical Technology and Applied Science at Virginia Polytechnic Institute and State University under the guidance of Prof. Michael W. Ellis. The first author was able to work on this project thanks to the sponsorship provided by the Mexican National Council on Science and Technology (CONACYT) and the University of Guanajuato.

References

[1] M. Rebai, M. Prat, Scale effect and two-phase flow in a thin hydrophobic porous layer. Application to water transport in gas diffusion layers of proton exchange membrane fuel cells, J. Power Sources 192 (2009) 534–543.
[2] Kyu-Jin Lee, Jin Hyun Nam, Charn-Jung Kim, Pore-network analysis of two-phase water transport in gas diffusion layers of polymer electrolyte membrane fuel cells, Electrochim. Acta 54 (2009) 1166–1176.
[3] Guangli He, Zongchang Zhao, Pingwen Ming, Abudula Abuliti, Caoyong Yin, A fractal model for predicting permeability and liquid water relative permeability in the gas diffusion layer (GDL) of PEMFCs, J. Power Sources 163 (2007) 846–852.
[4] Kyu-Jin Lee, Jin Hyun Nam, Charn-Jung Kim, Steady saturation distribution in hydrophobic gas-diffusion layers of polymer electrolyte membrane fuel cells: a pore-network study, J. Power Sources 195 (2010) 130–141.
[5] J. Park, X. Li, Multi-phase micro-scale flow simulation in the electrodes of a PEM fuel cell by lattice Boltzmann method, J. Power Sources 178 (2008) 248–257.
[6] C.Y. Wang, P. Cheng, A multiphase mixture model for multiphase, multi-component transport in capillary porous media I. Model development, Int. J. Heat Mass Transfer 39 (1996) 3607–3618.
[7] P. Cheng, C.Y. Wang, A multiphase mixture model for multiphase, multi-component transport in capillary porous media. II. Numerical simulation of

the transport of organic compounds in the subsurface, Int. J. Heat Mass Transfer 39 (1996) 3619–3632.
[8] Z.H. Wang, C.Y. Wang, K.S. Chen, Two-phase flow and transport in the air cathode of proton exchange membrane fuel cells, J. Power Sources 94 (2001) 40–50.
[9] Lixin You, Hongtan Liu, A two-phase flow and transport model for the cathode of PEM fuel cells, Int. J. Heat Mass Transfer 45 (2002) 2277–2287.
[10] Ugur Pasaogullari, Chao-Yang Wang, Two-phase transport and the role of microporous layer in polymer electrolyte fuel cells, Electrochim. Acta 49 (2004) 4359–4369.
[11] Ugur Pasaogullari, C.Y. Wang, Liquid water transport in gas diffusion layer of polymer electrolyte fuel cells, J. Electrochem. Soc. 15 (2004) 399–406.
[12] Ugur Pasaogullari, Chao-Yang Wang, Ken S. Chen, Two-phase transport in polymer electrolyte fuel cells with bilayer cathode gas diffusion media, J. Electrochem. Soc. 152 (2005) 1574–1582.
[13] Yun Wang, Suman Basu, Chao-Yang Wang, Modeling two-phase flow in PEM fuel cell channels, J. Power Sources 179 (2008) 603–617.
[14] Hyunchul Ju, Analyzing the effects of immobile liquid saturation and spatial wettability variation on liquid water transport in diffusion media of polymer electrolyte fuel cells (PEFCs), J. Power Sources 185 (2008) 55–62.
[15] Falin Chen, Min-Hsing Chang, Ping-Tso Hsieh, Two-phase transport in the cathode gas diffusion layer of PEM fuel cell with a gradient in porosity, Int. J. Hydrogen Energy 33 (2008) 2525–2529.
[16] N. Khajeh-Hosseini-Dalasm, Kazuyoshi Fushinobu, Ken Okazaki, Phase change in the cathode side of a proton exchange membrane fuel cell, J. Power Sources 195 (2010) 7003–7010.
[17] Hsiao-Kuo Hsuen, Ken-Ming Yin, A pseudo-phase-equilibrium approach for the calculation of liquid water saturation in the cathode gas diffuser of proton-exchange-membrane fuel cells, Int. J. Hydrogen Energy 36 (2011) 5487–5499.
[18] Wensheng He, Jung S. Yi, Trung Van Nguyen, Two-phase flow model of the cathode of PEM fuel cells using interdigitated flow fields, AIChE J. 46 (2000) 2053–2064.
[19] Dilip Natarajan, Trung Van Nguyen, A two-dimensional, two-phase, multi-component, transient model for the cathode of a proton exchange membrane fuel cell using conventional gas distributors, J. Electrochem. Soc. 148 (2001) 1324–1335.
[20] Jin Hyun Nam, Massoud Kaviany, Effective diffusivity and water-saturation distribution in single- and two-layer PEMFC diffusion medium, Int. J. Heat Mass Transfer 46 (2003) 4595–4611.
[21] T. Berning, N. Djilali, A 3D, multiphase, multicomponent model of the cathode and anode of a PEM fuel cell, J. Electrochem. Soc. 150 (2003) 1589–1598.
[22] Guangyu Lin, Wensheng He, Trung Van Nguyen, Modeling liquid water effects in the gas diffusion and catalyst layers of the cathode of a PEM fuel cell, J. Electrochem. Soc. 151 (2004) 1999–2006.
[23] N.P. Siegel, M.W. Ellis, D.J. Nelson, M.R. von Spakovsky, A two-dimensional computational model of a PEMFC with liquid water transport, J. Power Sources 128 (2004) 173–184.
[24] S.M. Senn, D. Poulikakos, Multiphase transport phenomena in the diffusion zone of a PEM fuel cell, J. Heat Transfer 127 (2005) 1245–1259.
[25] Guangyu Lin, Trung Van Nguyen, A two-dimensional two-phase model of a PEM fuel cell, J. Electrochem. Soc. 153 (2006) 372–382.
[26] M. Acosta, C. Merten, G. Eigenberger, H. Class, R. Helmig, B. Thoben, H. Mller-Steinhagen, Modeling non-isothermal two-phase multicomponent flow in the cathode of PEM fuel cells, J. Power Sources 159 (2006) 1123–1141.
[27] E.C. Kumbur, K.V. Sharp, M.M. Mench, On the effectiveness of Leverett approach for describing the water transport in fuel cell diffusion media, J. Power Sources 168 (2007) 356–368.
[28] J.E. Dawes, N.S. Hanspal, O.A. Family, A. Turan, Three-dimensional CFD modelling of PEM fuel cells: An investigation into the effects of water flooding, Chem Eng Sci 64 (2009) 2781–2794.
[29] Hua Meng, Multi-dimensional liquid water transport in the cathode of a PEM fuel cell with consideration of the micro-porous layer (MPL), Int. J. Hydrogen Energy 34 (2009) 5488–5497.
[30] Hua Meng, Numerical studies of liquid water behaviors in PEM fuel cell cathode considering transport across different porous layers, Int. J. Hydrogen Energy 35 (2010) 5569–5579.
[31] M. Srinivasarao, D. Bhattacharyya, R. Rengaswamy, S. Narasimhan, Parametric study of the cathode and the role of liquid saturation on the performance of a polymer electrolyte membrane fuel cell, a numerical approach, J. Power Sources 195 (2010) 6782–6794.
[32] Zhongying Shi, Xia Wang, Laila Guessous, Effect of compression on the water management of a proton exchange membrane fuel cell with different gas diffusion layers, J. Fuel Cell Sci. Technol. 7 (2010) 021012–021017.
[33] Stefano Cordiner, Simon Pietro Lanzani, Vincenzo Mulone, 3D effects of water-saturation distribution on polymeric electrolyte fuel cell (PEFC) performance, Int. J. Hydrogen Energy 36 (2011) 10366–10375.
[34] Chun-Hua Min, A novel three-dimensional, two-phase and non-isothermal numerical model for proton exchange membrane fuel cell, J. Power Sources 195 (2010) 1880–1887.
[35] K.H. Wong, K.H. Loo, Y.M. Lai, Siew-Chong Tan, Chi K. Tse, Treatment of two-phase flow in cathode gas channel for an improved one-dimensional proton exchange membrane fuel cell model, Int. J. Hydrogen Energy 36 (2011) 3941–3955.
[36] Bladimir Ramos-Alvarado, Joshua D. Sole, Abel Hernandez-Guerrero, Michael W. Ellis, Experimental characterization of the water transport properties of PEM fuel cells diffusion media, J. Power Sources 218 (2012) 221–232.
[37] COMSOL Multiphysics 4.0a Reference Guide.
[38] G. Velayutham, Effect of micro-layer PTFE on the performance of PEM fuel cell electrodes, Int. J. Hydrogen Energy 36 (2011) 14845–14850.
[39] Sehkyu Park, Jong-Won Lee, Branko N. Popov, Effect of PTFE content in microporous layer on water management in PEM fuel cells, J. Power Sources 177 (2008) 457–463.
[40] Jie-Cheng Tsai, Chien-Kung Lin, Effect of PTFE content in gas diffusion layer based on Nafion/PTFE membrane for low humidity proton exchange membrane fuel cell, J. Taiwan Inst. Chem. Eng. 42 (2011) 945–951.
[41] Gu-Gon Park, Young-Jun Sohn, Tae-Hyun Yang, Young-Gi Yoon, Won-Yong Lee, Chang-Soo Kim, Effect of PTFE contents in the gas diffusion media on the performance of PEMFC, J. Power Sources 131 (2004) 182–187.
[42] J.D. Sole, Investigation of water transport parameters and processes in the gas diffusion layer of PEM fuel cells, Doctoral dissertation, Virginia Polytechnic Institute and State University, 2008.